Cellular/Molecular

Visualization of Ca^{2+} Filling Mechanisms upon Synaptic Inputs in the Endoplasmic Reticulum of Cerebellar Purkinje Cells

Yohei Okubo,[1] Junji Suzuki,[1] Kazunori Kanemaru,[1] Naotoshi Nakamura,[2] Tatsuo Shibata,[2] and Masamitsu Iino[1]

[1]Department of Pharmacology, Graduate School of Medicine, The University of Tokyo, Tokyo 133-0033, Japan, and [2]Laboratory for Physical Biology, RIKEN Quantitative Biology Center, Kobe 650-0047, Japan

The endoplasmic reticulum (ER) plays crucial roles in intracellular Ca^{2+} signaling, serving as both a source and sink of Ca^{2+}, and regulating a variety of physiological and pathophysiological events in neurons in the brain. However, spatiotemporal Ca^{2+} dynamics within the ER in central neurons remain to be characterized. In this study, we visualized synaptic activity-dependent ER Ca^{2+} dynamics in mouse cerebellar Purkinje cells (PCs) using an ER-targeted genetically encoded Ca^{2+} indicator, G-CEPIA1*er*. We used brief parallel fiber stimulation to induce a local decrease in the ER luminal Ca^{2+} concentration ($[Ca^{2+}]_{ER}$) in dendrites and spines. In this experimental system, the recovery of $[Ca^{2+}]_{ER}$ takes several seconds, and recovery half-time depends on the extent of ER Ca^{2+} depletion. By combining imaging analysis and numerical simulation, we show that the intraluminal diffusion of Ca^{2+}, rather than Ca^{2+} reuptake, is the dominant mechanism for the replenishment of the local $[Ca^{2+}]_{ER}$ depletion immediately following the stimulation. In spines, the ER filled almost simultaneously with parent dendrites, suggesting that the ER within the spine neck does not represent a significant barrier to Ca^{2+} diffusion. Furthermore, we found that repetitive climbing fiber stimulation, which induces cytosolic Ca^{2+} spikes in PCs, cumulatively increased $[Ca^{2+}]_{ER}$. These results indicate that the neuronal ER functions both as an intracellular tunnel to redistribute stored Ca^{2+} within the neurons, and as a leaky integrator of Ca^{2+} spike-inducing synaptic inputs.

Key words: calcium; endoplasmic reticulum; inositol 1,4,5-trisphosphate; metabotropic glutamate receptor; Purkinje cell

Significance Statement

Ca^{2+} is a key messenger that regulates neuronal functions in the brain. Although the endoplasmic reticulum (ER) plays indispensable roles as a source and sink of Ca^{2+}, technical difficulties have impeded the analysis of Ca^{2+} dynamics within the ER. In this study, we have used a genetically encoded ER Ca^{2+} indicator to visualize Ca^{2+} dynamics within the neuronal ER. We found that Ca^{2+}-mobilizing synaptic inputs locally decreased the ER Ca^{2+} concentration, followed by Ca^{2+} replenishment by intraluminal Ca^{2+} diffusion throughout the ER of dendrites and spines. Furthermore, Ca^{2+} spike-inducing synaptic inputs cumulatively increased the Ca^{2+} content of the ER. Thus, our study indicates that the ER functions both as a tunnel to redistribute stored Ca^{2+} and as a leaky integrator of synaptic inputs.

Introduction

Understanding the dynamics and regulatory mechanisms of the endoplasmic reticulum (ER) luminal free Ca^{2+} concentration ($[Ca^{2+}]_{ER}$) is critical for understanding the function of the ER in neurons. In various types of cells, the ER is a major intracellular Ca^{2+} store and plays a crucial role in intracellular Ca^{2+} signaling, serving as both a source and a sink of Ca^{2+}. In central neurons, synaptic inputs may evoke Ca^{2+} release from the ER through two types of Ca^{2+} release channels, inositol trisphosphate (IP_3) receptors and ryanodine receptors, thereby regulating a variety of physiological and pathophysiological events (Berridge, 1998; Verkhratsky, 2005). As the driving force for Ca^{2+} mobilization, $[Ca^{2+}]_{ER}$ is a critical factor for ER-mediated Ca^{2+} signaling. Al-

Received Sept. 17, 2015; revised Oct. 15, 2015; accepted Oct. 25, 2015.

Author contributions: Y.O. and M.I. designed research; Y.O., J.S., K.K., and N.N. performed research; J.S. and K.K. contributed unpublished reagents/analytic tools; Y.O., N.N., and T.S. analyzed data; Y.O. and M.I. wrote the paper.

This work was supported by grants from the Ministry of Education, Culture, Sports, Science and Technology, Japan; Takeda Science Foundation; and The Tokyo Society of Medical Sciences. We thank Y. Kawashima for technical assistance.

The authors declare no competing financial interests.

Correspondence should be addressed to Masamitsu Iino, Department of Pharmacology, Graduate School of Medicine, The University of Tokyo, 7-3-1 Hongo, Bunkyo-ku, Tokyo 113–0033, Japan. E-mail: iino@m.u-tokyo.ac.jp.

DOI:10.1523/JNEUROSCI.3487-15.2015

 0270-6474/15/3515837-10$15.00/0

though cell-wide depletion and replenishment of Ca^{2+} in the neuronal ER have been visualized previously (Fujiwara et al., 2001; Solovyova et al., 2002; Rodriguez-Garcia et al., 2014), the relationship between synaptic inputs and Ca^{2+} dynamics within the ER remains poorly understood. Previous studies (Brorson et al., 1991; Garaschuk et al., 1997; Finch and Augustine, 1998; Fiorillo and Williams, 1998; Stutzmann et al., 2003; Power and Sah, 2005; Hong and Ross, 2007; Hartmann et al., 2014) have shown that, in neurons, voltage-gated Ca^{2+} channels induce an influx of Ca^{2+} that subsequently enhances Ca^{2+} release. Although this priming effect is thought to increase the ER Ca^{2+} content by activating the sarcoplasmic/endoplasmic reticulum Ca^{2+}-ATPase (SERCA), the actual Ca^{2+} concentration of the ER has not been directly examined, due in part to the lack of appropriate technologies for monitoring ER Ca^{2+} dynamics. This limitation represents a major obstacle in studying the function of the neuronal ER.

In earlier studies (Garaschuk et al., 1997), Ca^{2+} concentration within the ER could be estimated only by indirect measurement of changes in cytoplasmic Ca^{2+} concentration in response to activation of Ca^{2+} release from the ER. However, interpretation of such results has been inevitably complicated by changes in the Ca^{2+} mobilization mechanisms themselves, and has therefore prompted the development of technologies to directly measure Ca^{2+} dynamics in the ER. One such method is the use of small molecular Ca^{2+} indicators; however, difficulty in targeting them to the lumen of the ER has limited their application in intact neurons (Fujiwara et al., 2001; Solovyova et al., 2002). In contrast, genetically encoded Ca^{2+} indicators (GECIs) can be targeted to the ER by tagging with appropriate ER retention signals. This capability has been exploited to develop a variety of GECIs for the visualization of ER Ca^{2+} dynamics (Miyawaki et al., 1997; Palmer et al., 2004; Ishii et al., 2006; Tang et al., 2011; Bonora et al., 2013; Rodriguez-Garcia et al., 2014; Wu et al., 2014). To improve the spatiotemporal resolution of GECIs, we recently developed a series of calcium-measuring organelle-entrapped protein indicators (CEPIAs), which are GECIs that can provide high-resolution visualization of ER Ca^{2+} dynamics in various types of cells, including neurons (Suzuki et al., 2014).

In this study, we expressed the ER-targeted genetically encoded Ca^{2+} indicator G-CEPIA1*er* in mouse cerebellar Purkinje cells (PCs), which possess a well developed ER with a high density of IP_3 receptors (Martone et al., 1993; Sharp et al., 1993). We then evoked synaptic inputs from parallel fibers (PFs) and climbing fibers (CFs), and observed how the ER network within the PCs responded to those inputs. Collectively, these ER Ca^{2+} visualization studies provide important new insights into synaptically evoked $[Ca^{2+}]_{ER}$ dynamics.

Materials and Methods

Gene construction. For PC-specific expression of G-CEPIA1*er*, we produced a Sindbis virus (Okubo et al., 2001, 2004; Suzuki et al., 2014). The pSinRep5 subcloning version of G-CEPIA1*er* was used as the template for *in vitro* transcription using SP6 RNA polymerase (Ambion). The RNA transcript and the helper RNA from DH(26S) cDNA template (Invitrogen) were cotransfected into BHK cells by electroporation. Twenty-four hours after transfection, the culture medium containing the infectious particles was harvested. Sindbis virus encoding G-GECO1.1 (Zhao et al., 2011) for the cytoplasmic Ca^{2+} measurement was also produced by the same procedure.

Infection of PCs and preparation of cerebellar slices. All animal experiments were performed in accordance with the regulations and guidelines of the Institutional Animal Care and Use Committee at The University of Tokyo and were approved by the institutional review committees of the Graduate School of Medicine, University of Tokyo. Male C57BL/6 mice (postnatal day 21–27) were deeply anesthetized with pentobarbital, and the surface of cerebellar lobule 6 adjacent to the midline was exposed by removing the cranium and dura. The tip of a glass pipette was backfilled with the viral solution. The glass pipette was then inserted into the cerebellum, and 1 μl of viral solution was delivered at a rate of 200 nl/min using a micropump (Legato 130, KD Scientific). Twenty-three to 26 h after virus injection, parasagittal cerebellar slices (250 μm thickness) were prepared as described previously (Edwards et al., 1989). Slices were incubated in a holding chamber containing artificial CSF (ACSF) bubbled with 95% O_2 and 5% CO_2 at 35°C for 1 h and then returned to 23°C. ACSF for slicing and incubation contained the following (in mM): 125 NaCl, 2.5 KCl, 2 $CaCl_2$, 1 $MgSO_4$, 1.25 NaH_2PO_4, 26 $NaHCO_3$, and 20 glucose.

Imaging. Imaging was performed with a two-photon microscope (TSC MP5, Leica) that was equipped with a water-immersion objective (25×, numerical aperture, 0.95; HCS IR APO, Leica) and a Ti:sapphire laser (MaiTai DeepSee, Spectra Physics). Slices were transferred to a recording chamber under microscope, continuously perfused with ACSF bubbled with 95% O_2 and 5% CO_2, and supplemented with 10 μM bicuculline (Tocris Bioscience) to block spontaneous IPSCs. The excitation wavelength was 900–920 nm. Emitted fluorescence was filtered using an infrared-ray cutting filter, separated by a 560 nm dichroic mirror and detected with photomultiplier tubes. A 500–550 nm barrier filter and a 600 nm long-pass filter were used for the green and red channels, respectively. Data were acquired with time-lapse XY-scan mode (8–10 Hz for PF-induced responses and 1–2 Hz for CF-induced responses). For higher-frequency sampling, line-scan mode (200–400 Hz) was applied. For the focal stimulation of PFs, five square pulses (0.1 ms duration) were applied at 100 Hz through stimulation pipettes (3–6 μm tip diameter) filled with ACSF and placed just above the imaging field. The stimulation intensity was adjusted within 2–5 V to induce G-CEPIA1*er* responses confined within narrow dendritic segments (~5–10 μm in diameter of detectable signals). During PF simulation with 2× intensity (i.e., 4–10 V), 2,3-dihydroxy-6-nitro-7-sulfonyl-benzo[*f*]quinoxaline (NBQX) was included in ACSF to avoid the excessive AMPAR-dependent Ca^{2+} influx and its possible effect on ER Ca^{2+} dynamics. For CF stimulation, square pulses (0.1 ms, 0–20 V) were applied at 1 Hz through stimulation pipettes placed on the granule cell layer adjacent to the soma of the PC of interest. For the local application of 3,5-dihydroxyphenylglycine (DHPG), DHPG was pressure ejected (1 mM, 50 ms, 10–30 psi) using a fine pipette (<1 μm tip diameter) placed 5–15 μm above the dendrite of G-GECO1.1-expressing PCs. Bicuculline, (*S*)-(+)-α-amino-4-carboxy-2-methylbenzeneacetic acid (LY367385), NBQX, cyclopiazonic acid (CPA), and DHPG were obtained from Tocris Bioscience. Drugs other than DHPG were dissolved in ACSF and administered through the perfusion system of the recording chamber. Experiments were performed at room temperature (RT; 22–24°C), unless otherwise stated.

Data analysis. Data were analyzed using ImageJ software. Fluorescence intensities were corrected for background fluorescence by measuring a nonfluorescent area. When necessary, photobleaching was corrected using a linear fit to the fluorescence intensity change in nonstimulated area. The fractional change in fluorescence intensity from the basal level ($\Delta F/F_0$) was analyzed. The amplitude of PF-induced G-CEPIA1*er* responses was defined as the maximum decrease in $\Delta F/F_0$ after PF stimulation. The amplitude of CF-induced G-CEPIA1*er* responses was defined as the maximum increase in $\Delta F/F_0$ during 20 pulses of CF stimulation. The amplitude of DHPG-induced G-GECO1.1 responses was defined as the maximum increase in $\Delta F/F_0$. For the measurement of amplitude, time courses of $\Delta F/F_0$ were smoothed by a moving average with a five-frame window. The amplitude shown in Figure 2*E* is defined as the average of $\Delta F/F_0$ within the 1 s (for X-rhod-1) or 5 s (for G-CEPIA1*er*) time windows, starting from the end of PF stimulation. For the measurement of half recovery time ($t_{1/2}$), the decay phase of PF-induced G-CEPIA1*er* response was fitted with the exponential function, including a linear component. The time point (with $t = 0$ set at the end of PF stimulation) at which $\Delta F/F_0$ recovered by half was calculated using the fitted function and measured amplitude. Time to peak was defined as the time between the end of PF stimulation and the point of maximum decrease in $\Delta F/F_0$, the location of which was determined after data smoothing using 5 data

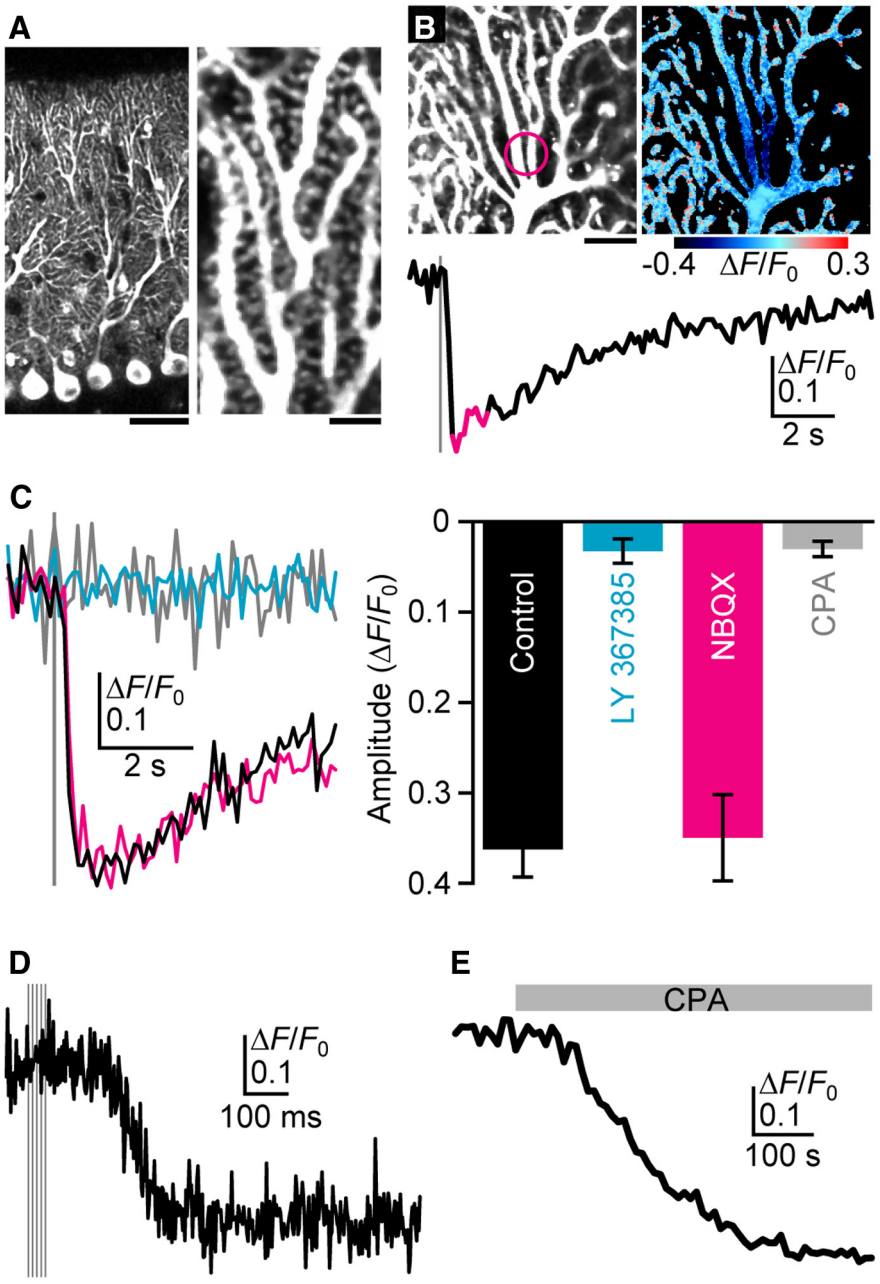

Figure 1. Visualization of PF-induced ER Ca^{2+} dynamics. ***A***, G-CEPIA1*er*-expressing PCs in the cerebellar slice. Scale bars: left, 40 μm; right, 4 μm. ***B***, Representative time course of mean $\Delta F/F_0$ values within the dendritic segment (indicated by the circle in the top left image) upon PF inputs (five stimuli at 100 Hz, gray vertical line) indicates PF-induced ER Ca^{2+} dynamics in PCs. The pseudo-color image represents the average of 10 consecutive frames (indicated as magenta in the time course of $\Delta F/F_0$). Scale bar, 10 μm. ***C***, Pharmacological characterization of PF-induced ER Ca^{2+} dynamics. G-CEPIA1*er* responses upon PF inputs (five stimuli at 100 Hz, gray vertical line) in the control condition (black); in the presence of LY367385 (100 μM, cyan) or NBQX (10 μM, magenta); or after the depletion of ER with CPA (50 μM, gray) are shown. Amplitude is defined as the maximum decrease in $\Delta F/F_0$ within the 3 s time window after PF stimulation. $n = 7$–12 (mean ± SEM). ***D***, High-frequency measurement of PF-induced G-CEPIA1*er* response. Time course of $\Delta F/F_0$ upon PF inputs (five stimuli at 100 Hz, gray vertical line) was measured by the line-scan imaging of the dendrite. ***E***, CPA-induced ER depletion. The application of CPA (50 μM, gray) decreased G-CEPIA1*er* fluorescence with the $\Delta F/F_0$ amplitude of 0.43 ± 0.021 (mean ± SEM, $n = 6$).

point moving average. To avoid overestimation of the time to peak, we discarded data if the $\Delta F/F_0$ trace had no recognizable trough at distal locations. To analyze the diffusional dynamics in PF-induced G-CEPIA1*er* responses, we manually determined the central point of the response by carefully inspecting the spatial distribution of $\Delta F/F_0$ 1–2 s after PF stimulation. If responses covered more than one dendritic branch, the central points were set in each dendrite. Distance was measured along the skeletonized dendrites that consist of the manually delineated centerlines of dendrites.

Fluorescence recovery after photobleaching (FRAP) experiments. G-CEPIA1*er* was bleached by the illumination of an excitation laser (900–920 nm) within a 5-μm-diameter circle. Amplitude was defined as $\Delta F/F_0$ just after the end of photobleaching. For the measurement of $t_{1/2}$, the recovery phase of G-CEPIA1*er* fluorescence was fitted with the exponential function, including a linear component. The time point (with $t = 0$ set at the end of photobleaching) at which $\Delta F/F_0$ recovered by half was calculated using the fitted function and measured amplitude.

Patch-clamp experiments. Whole-cell patch-clamp experiments were performed for the simultaneous visualization of cytoplasmic Ca^{2+} concentration ($[Ca^{2+}]_{cyt}$) and $[Ca^{2+}]_{ER}$ dynamics, and the recording of CF-induced EPSPs. The resistances of patch pipettes were 4–7 MΩ when filled with the intracellular solution containing the following (in mM): 130 K-gluconate, 4 $MgCl_2$, 4 Na_2ATP, 0.4 Na_2 GTP, 10 sodium phosphocreatine, 3 sodium L-ascorbate, and 10 HEPES, pH 7.3, adjusted with KOH. The intracellular solution also contained 0.1 mM X-rhod-1 (Anaspec) or 0.2 mM EGTA. For the simultaneous visualization of $[Ca^{2+}]_{cyt}$ and $[Ca^{2+}]_{ER}$ dynamics, X-rhod-1 was introduced to the cytoplasm of G-CEPIA1*er*-expressing PCs via patch pipettes. PCs were held at −60 to −70 mV with an EPC-9 patch-clamp amplifier (HEKA) using the voltage-clamp mode. NBQX was included in ACSF to isolate ER-mediated $[Ca^{2+}]_{cyt}$ responses by inhibiting AMPAR-dependent Ca^{2+} influx. CF-induced EPSPs were recorded with an EPC-9 patch-clamp amplifier using the current-clamp mode. The intensity of CF stimulation pulses was set just above the threshold to induce CF-induced EPSPs, and the intensity just below the threshold was applied for nonspiking controls. The on-line data acquisition and off-line analysis of data were performed using PULSE software (HEKA).

Modeling of ER Ca^{2+} dynamics. The time evolution of ER Ca^{2+} concentration after PF-induced local depletion was modeled by the following one-dimensional reaction–diffusion equation:

$$\frac{du}{dt} = D\nabla^2 u - k(u - u_0).$$

The equation describes lateral diffusion of ER Ca^{2+} and SERCA-dependent Ca^{2+} uptake, and u (in μM), u_0 (in μM), D (in $\mu m^2/s$), and k (in s) denote ER Ca^{2+} concentration, basal ER Ca^{2+} concentration, the diffusion coefficient of Ca^{2+}, and SERCA activity, respectively. The term $k(u - u_0)$ shows the contribution of ER Ca^{2+} leak channels and SERCA Ca^{2+} pumps. Since $[Ca^{2+}]_{cyt}$ is nearly constant during the ER Ca^{2+} recovery phase (see Fig. 2*D*), SERCA activity, which depends on $[Ca^{2+}]_{cyt}$, was set to be constant in the model. Boundary conditions at the end of dendrites were chosen to be either Dirichlet (equal to basal concentration) or Neumann (zero flux) according to the actual dendrite

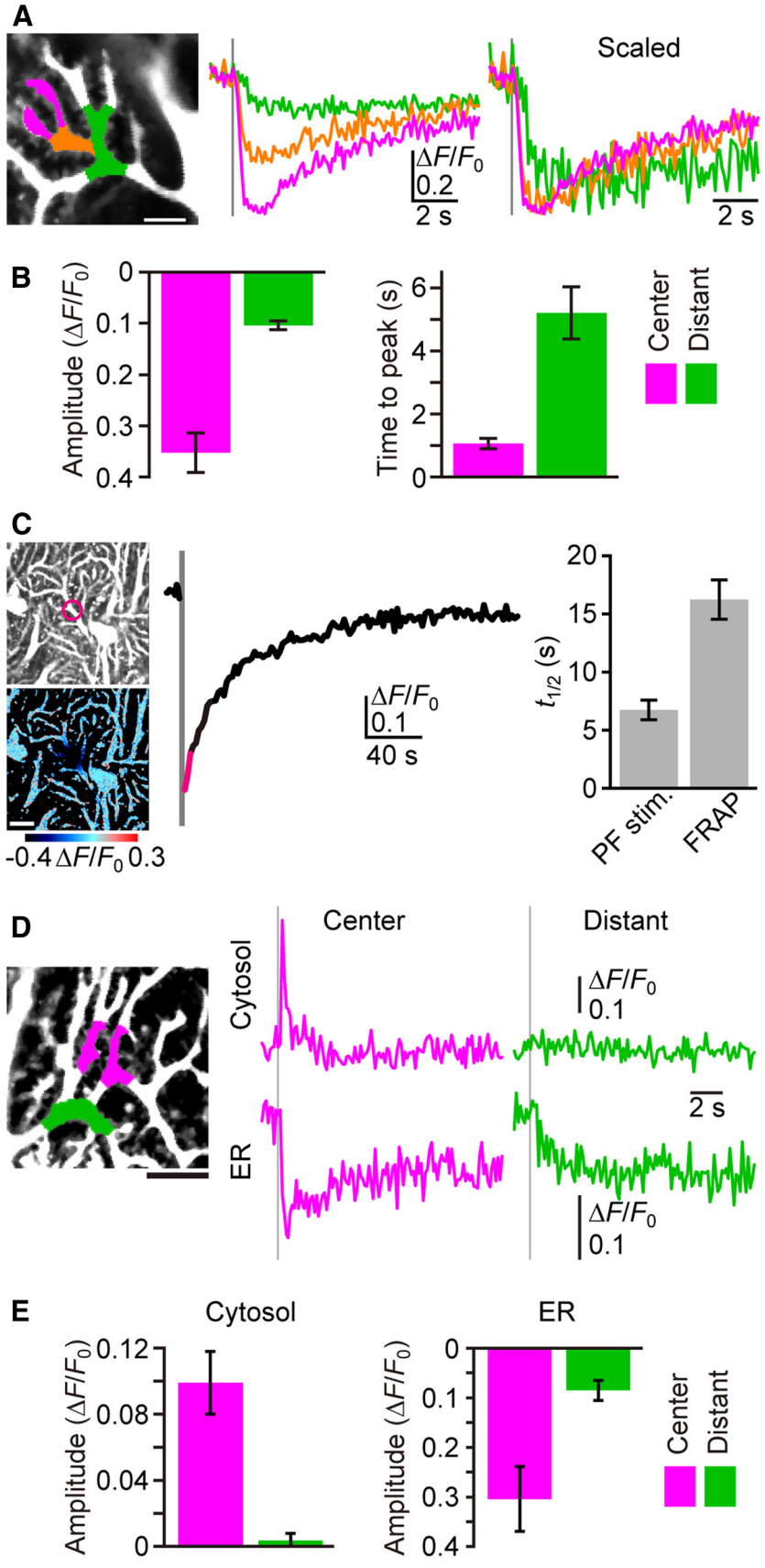

Figure 2. Lateral diffusion of Ca^{2+} within ER. ***A***, Lateral diffusion of luminal Ca^{2+}, as suggested by the wave-like propagation of the G-CEPIA1*er* response. Dendritic segments and corresponding $\Delta F/F_0$ traces upon PF inputs (five stimuli at 100 Hz, gray vertical line) were color coded (magenta, orange, and green). Scale bar, 5 μm. ***B***, Summary of differences between the central and distant segment of PF-induced responses. Center (magenta) was defined as dendritic segments within 5 μm from the central point, and distant (green) was defined as segments >7 μm distal to the central point (for details, see Materials and Methods). $n = 8$ (mean ± SEM). ***C***, Time course of $\Delta F/F_0$ within the dendritic segment (indicated by the circle in the left image) indicates the decrease in fluorescence upon photobleaching (gray vertical line) and the subsequent recovery (FRAP). The pseudocolor image that is the average of three consecutive frames (indicated as magenta in the time course of $\Delta F/F_0$) shows local fluorescence decrease. $t_{1/2}$ upon PF inputs is indicated for comparison in the right bar graph. $n = 10$ (mean ± SEM). Scale bar, 10 μm. ***D***, Cytosolic and ER Ca^{2+} dynamics visualized by introducing X-rhod-1 to the cytosol of G-CEPIA1*er*-expressing PCs. Time courses of $\Delta F/F_0$ for X-rhod-1 (cytosol) and G-CEPIA1*er* (ER) within the central segment (magenta) or the distant segment (green) upon PF inputs (five stimuli at 100 Hz, gray vertical line) are shown. NBQX (10 μM) was applied to isolate mGluR1-dependent responses. Scale bar, 10 μm. ***E***, Summary of differences between the central and distant segments of PF-induced cytosolic and ER Ca^{2+} responses. Amplitude is defined as the average of $\Delta F/F_0$ within the 1 s (for cytosol) or 5 s (for ER) time window starting from the end of PF stimulation. $n = 5$ (mean ± SEM).

geometry. Diffusion in a tube of abruptly changing diameter can be described by a one-dimensional diffusion equation with a constant diffusion coefficient (Berezhkovskii et al., 2009; Makhnovskii et al., 2010). Borrowing from this theory, we reduced the diffusion through the dendritic branching (see Fig. 3*A*) to one-dimensional diffusion with alternating diameter as follows. We aligned and merged branches along the distance from the central point of response, and let the merged segments possess the pump/leak coefficient (k) multiplied by the number of merged branches. The Ca^{2+} diffusion coefficient (D) was assumed to be constant throughout the one-dimensional structure. The simulated ER Ca^{2+} concentration u was converted to G-CEPIA1*er* fluorescence F using the following equation, which was described previously (Suzuki et al., 2014):

$$F = F_{min} + (F_{max} - F_{min}) \times u^n/(u^n + K_d^n),$$

and was compared with experimental data. The following values from Suzuki et al. (2014) were used: The maximum fractional change in the fluorescence intensity (F_{max}/F_{min}) = 4.7, K_d = 672 μM, n = 1.95. For Figure 3*A*, the following values were selected to fit the model to the data: $D = 8.4070$, $k = 0.0146$, $u_0 = 995.6$. These values were determined using an automated trial-and-error, parameter-optimizing program written in MATLAB version 8.3. The basal ER Ca^{2+} concentration (u_0 = 995.6 μM) that we obtained was comparable to the resting $[Ca^{2+}]_{ER}$ measured in other cell types in our recent study (Suzuki et al., 2014).

Results

Visualizing synaptically evoked ER Ca^{2+} dynamics with G-CEPIA1*er*

We used Sindbis virus to express G-CEPIA1*er* in PCs and a two-photon microscope to image its expression in acute cerebellar slices, first focusing on

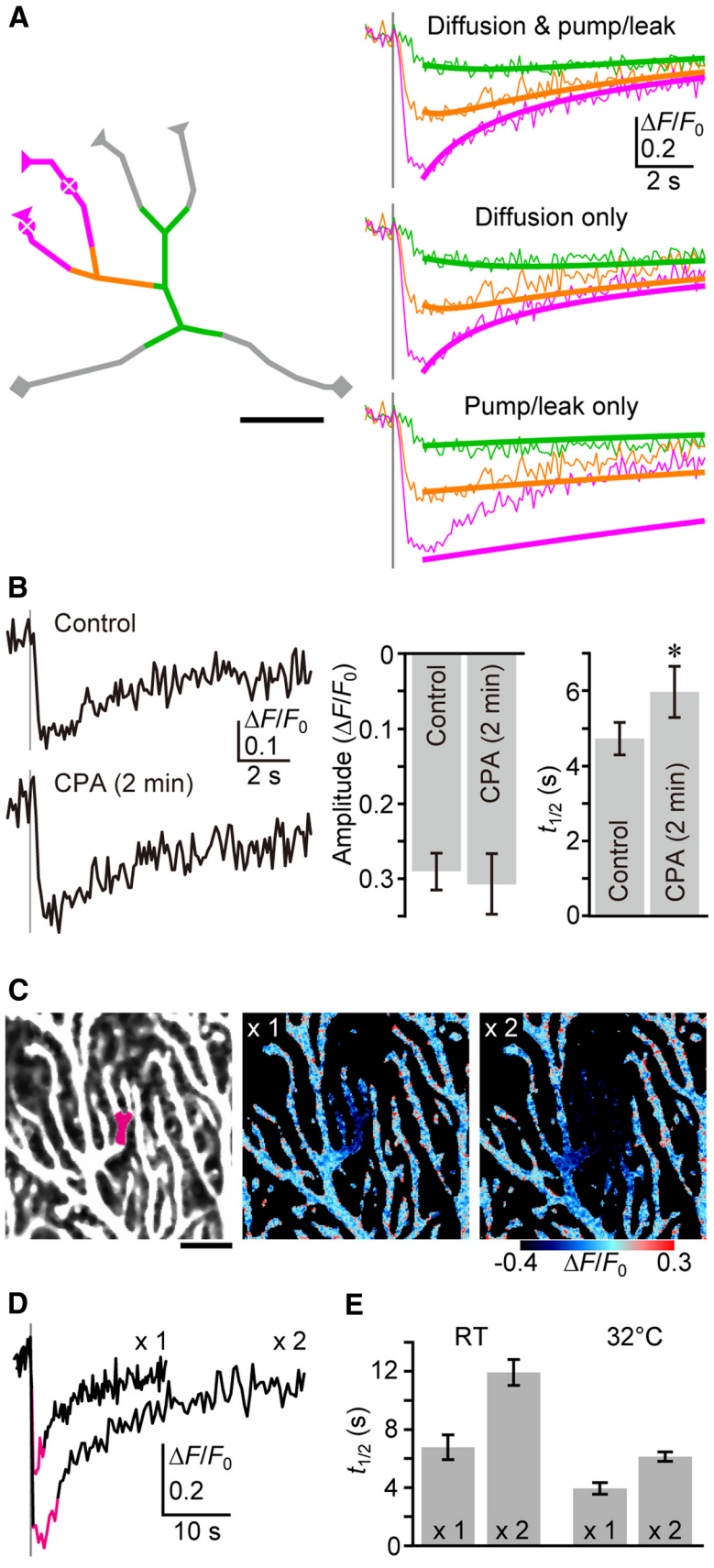

Figure 3. Contribution of intraluminal Ca^{2+} diffusion to ER refilling after PF inputs. ***A***, Numerical simulation of ER Ca^{2+} dynamics during the refilling period. Left, The actual dendritic structure shown in Figure 2*A* was manually skeletonized, and reaction-diffusion modeling performed. The triangles on the terminals indicate the dead-end boundary, while the squares indicate the open-end boundary. Dendritic segments for the calculation of $\Delta F/F_0$ were indicated by colors, as in Figure 2*A*. The central dendrites (Fig. 1; see Fig. 4, data for spines). We observed G-CEPIA1*er* expression throughout dendrites and spines (Fig. 1*A*), which was consistent with earlier reports on the distribution pattern of the ER in PCs (Martone et al., 1993; Sharp et al., 1993). It has been well documented that PF inputs induce metabotropic glutamate receptor 1 (mGluR1)-IP_3-mediated local Ca^{2+} release from the ER, which increases the $[Ca^{2+}]_{cyt}$ in PC dendrites and spines (Finch and Augustine, 1998; Takechi et al., 1998; Okubo et al., 2004). Indeed, in response to focal PF stimulation with a physiologically relevant stimulation pattern (five pulses at 100 Hz), we observed a transient decrease in G-CEPIA1*er* fluorescence intensity in dendrites and spines confined within a narrow segment [Fig. 1*B*; preliminary observations were shown in our recent report (Suzuki et al., 2014)].

We next pharmacologically manipulated the intracellular signaling mechanism involved in PF-induced ER Ca^{2+} dynamics. First, we showed that, as expected, the application of LY367385 (Fig. 1*C*, cyan), an mGluR1 antagonist, blocked the PF-induced G-CEPIA1*er* response that results from mGluR1-IP_3-mediated Ca^{2+} mobilization at PF–PC synapses (Finch and Augustine, 1998; Takechi et al., 1998; Okubo et al., 2004). Furthermore, using highly resolved temporal measurements of the PF-induced G-CEPIA1*er* response, we demonstrated that immediately following PF stimula-

←

points of response (the bottom points of the initial distribution of $[Ca^{2+}]_{ER}$) were marked. Scale bar, 5 μm. Right, The recovery phase of G-CEPIA1*er* response was fitted to the model. $\Delta F/F_0$ traces (thin lines) are color coded as for those shown in Figure 2*A*. The reaction-diffusion model faithfully reproduced the recovery time course in each dendritic segment (thick lines). The calculated effective diffusion coefficient of Ca^{2+} in ER lumen was 8.4 $\mu m^2/s$. Simulated results for no diffusion and no pump/leak were produced by resetting the each coefficient to 0 after data fitting. For details, see Materials and Methods. ***B***, The effect of short-term treatment with CPA (50 μM, 2 min) on the replenishment rate. Representative time courses of $\Delta F/F_0$ upon PF inputs (five stimuli at 100 Hz, gray vertical line), and the summarized bar graph for $\Delta F/F_0$ amplitude and $t_{1/2}$ are shown. $t_{1/2}$ is the time point at which $\Delta F/F_0$ recovered by half. $n = 7$ (mean ± SEM). $^*p = 0.00581$, *t* test. ***C***, The area of PF-induced $[Ca^{2+}]_{ER}$ decrease was enlarged by a twofold increase of stimulation intensity (indicated as ×2). The pseudo-color images are the averages of 10 consecutive frames (indicated as magenta in $\Delta F/F_0$ traces in ***D***). Scale bar, 10 μm. ***D***, Representative time courses of $\Delta F/F_0$ within the dendritic segment (indicated by magenta in the top left image in ***C***) upon PF inputs (five stimuli at 100 Hz, gray vertical line). ***E***, The summarized bar graph for $t_{1/2}$ under RT or 32°C. ($n = 8$ each, mean ± SEM).

tion, there was a ~200 ms period of latency, which is consistent with previous observations of mGluR1-IP_3-mediated cytoplasmic Ca^{2+} transients (Finch and Augustine, 1998; Takechi et al., 1998; Okubo et al., 2004; Fig. 1*D*). This result indicates that the Ca^{2+} dissociation kinetics of G-CEPIA1*er* is fast enough to follow the synaptically evoked $[Ca^{2+}]_{ER}$ dynamics. In contrast, the application of NBQX (Fig. 1*C*, magenta), an AMPAR antagonist, had no effect on ER Ca^{2+} dynamics. On the other hand, the application of CPA, a SERCA inhibitor, induced slow depletion of ER Ca^{2+} (Fig. 1*E*), followed by abolishment of the G-CEPIA1*er* response to PF stimulation (Fig. 1*C*, gray). In conclusion, G-CEPIA1*er* enabled the visualization of ER Ca^{2+} dynamics confined to the vicinity of PF inputs in PCs, which allowed us to analyze the molecular mechanisms for refilling the ER with Ca^{2+}, following synaptically evoked Ca^{2+} mobilization in neurons.

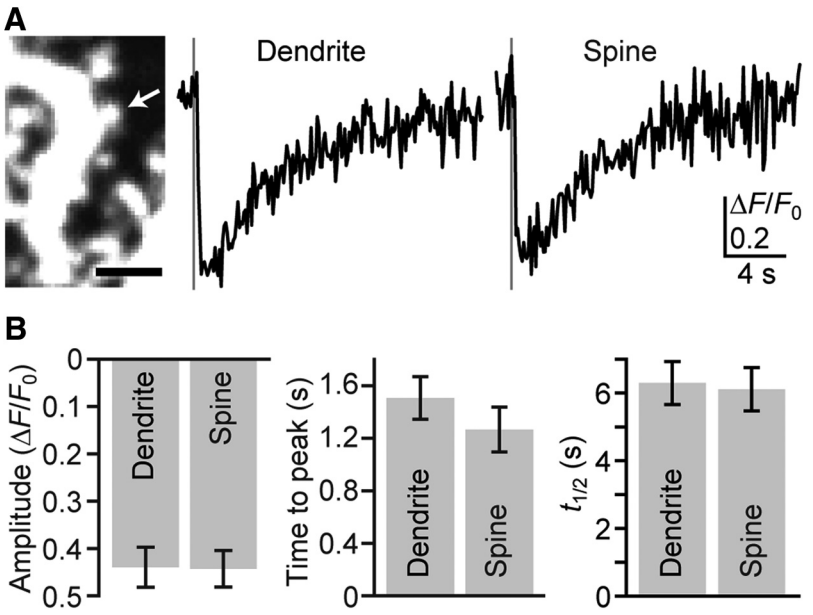

Figure 4. Simultaneous replenishment of Ca^{2+} in the ER of spines and parent dendrites. ***A***, Kinetics of PF-induced responses compared between spines and their parent dendrites. Representative time courses of $\Delta F/F_0$ within the spine (indicated by the arrow in the left image) and its parent dendrite upon PF inputs (five stimuli at 100 Hz, gray vertical line) are shown. Scale bar, 2 μm. ***B***, Summary of the $\Delta F/F_0$ amplitude, time to peak, and $t_{1/2}$ in spines and their parent dendrites ($n = 13$ pairs, mean ± SEM).

Lateral diffusion of Ca^{2+} within the ER

After Ca^{2+} is depleted cell wide throughout the ER, SERCA-dependent Ca^{2+} uptake is likely a crucial mechanism for refilling. However, as shown in Figure 1*B*, local decreases in $[Ca^{2+}]_{ER}$ induced by PF inputs recovered far faster than recovery in cell-wide ER depletion experiments conducted on neurons (~1 min; Garaschuk et al., 1997; Solovyova et al., 2002; Hartmann et al., 2014). Therefore, it is possible that the rapid refilling of ER Ca^{2+} following a PF input occurs through the diffusion of intraluminal Ca^{2+} from unstimulated segments to depleted segments of the ER, as suggested by studies in other cell types (Mogami et al., 1997; Choi et al., 2006; Petersen and Verkhratsky, 2007).

Using our newly developed ER Ca^{2+} imaging technology, we were able to directly examine the role of intraluminal Ca^{2+} diffusion in recovery. We divided dendrites into segments according to their distance from the PF stimulation input site, and compared the PF-induced $[Ca^{2+}]_{ER}$ responses of each segment. The analysis showed that the responses became smaller in magnitude and slower in onset according to the distance of the segment from the input site, which is consistent with a diffusional mechanism (Fig. 2*A*,*B*). The observed $[Ca^{2+}]_{ER}$ dynamics did not appear to be the result of the diffusion of G-CEPIA1*er* itself, because FRAP of G-CEPIA1*er* within narrow dendritic segments resulted in much slower $t_{1/2}$ of fluorescence intensity than that of the Ca^{2+} signal after PF inputs (Fig. 2*C*).

Alternatively, the smaller and slower $[Ca^{2+}]_{ER}$ dynamics in the distant dendritic segments can be explained if IP_3 generated at the input site reaches the ER in the distant segments by diffusion through the cytosol to induce delayed release of Ca^{2+}. To examine this possibility, we performed simultaneous cytosolic and ER Ca^{2+} imaging by introducing X-rhod-1, a red color Ca^{2+} indicator, to the cytosol of G-CEPIA1*er*-expressing PCs, using a patch pipette (Fig. 2*D*). We observed that immediately beneath the PF stimulation electrode, where $[Ca^{2+}]_{ER}$ decreased rapidly, there was a transient increase in cytosolic Ca^{2+} (Fig. 2*D*,*E*). In the distant segments, however, the delayed decrease in $[Ca^{2+}]_{ER}$ was not accompanied by a detectable increase in cytosolic Ca^{2+} (Fig. 2*D*,*E*). These results indicate that Ca^{2+} is not released from the ER in the distant segments, and argue against the alternative possibility that the diffusion of IP_3 caused delayed $[Ca^{2+}]_{ER}$ dynamics in the distant dendritic segments.

Diffusion-dependent ER refilling of Ca^{2+} after PF-induced Ca^{2+} mobilization

To estimate the extent to which intraluminal Ca^{2+} diffusion contributes to the replenishment of Ca^{2+} within the ER following local decreases in $[Ca^{2+}]_{ER}$, we performed numerical simulations of ER Ca^{2+} dynamics. Specifically, we modeled and solved a one-dimensional reaction-diffusion equation describing lateral diffusion of Ca^{2+} within the modeled dendritic structure, as well as Ca^{2+} pump-dependent Ca^{2+} uptake and leak from the ER to the cytosol (Fig. 3*A*). Data fitting using the equation faithfully reproduced the recovery dynamics of G-CEPIA1*er* fluorescence and indicated the effective diffusion coefficient of Ca^{2+} within the ER lumen to be 8.4 $\mu m^2/s$ (see Materials and Methods). We confirmed that lateral diffusion is critical by observing a significant slowing of $[Ca^{2+}]_{ER}$ recovery at the central segment when no diffusion was allowed in the simulation (Fig. 3*A*, bottom). In contrast, we showed that Ca^{2+} uptake provides a relatively minor contribution by a simulation where Ca^{2+} pump and leak activity was not allowed (Fig. 3*A*, middle).

We next used CPA to experimentally validate the numerical simulations. After the application of CPA to G-CEPIA1*er*-expressing PCs, we observed a decrease in $[Ca^{2+}]_{ER}$ after a short lag time (Fig. 1*E*), indicating that CPA acts by immediately inhibiting SERCA. Treating PCs with CPA for 2 min induced a small but significant decrease in G-CEPIA1*er* fluorescence [mean (±SEM) fractional decrease = 0.087 ± 0.019; $n = 7$], indicating that SERCA was inhibited by CPA within 2 min of application. We then measured the $t_{1/2}$ of PF-induced G-CEPIA1*er* responses before and 2 min after CPA treatment. CPA treatment resulted in only a slight increase in $t_{1/2}$ (Fig. 3*B*). These results are consistent with the prediction of our numerical simulation that there is a

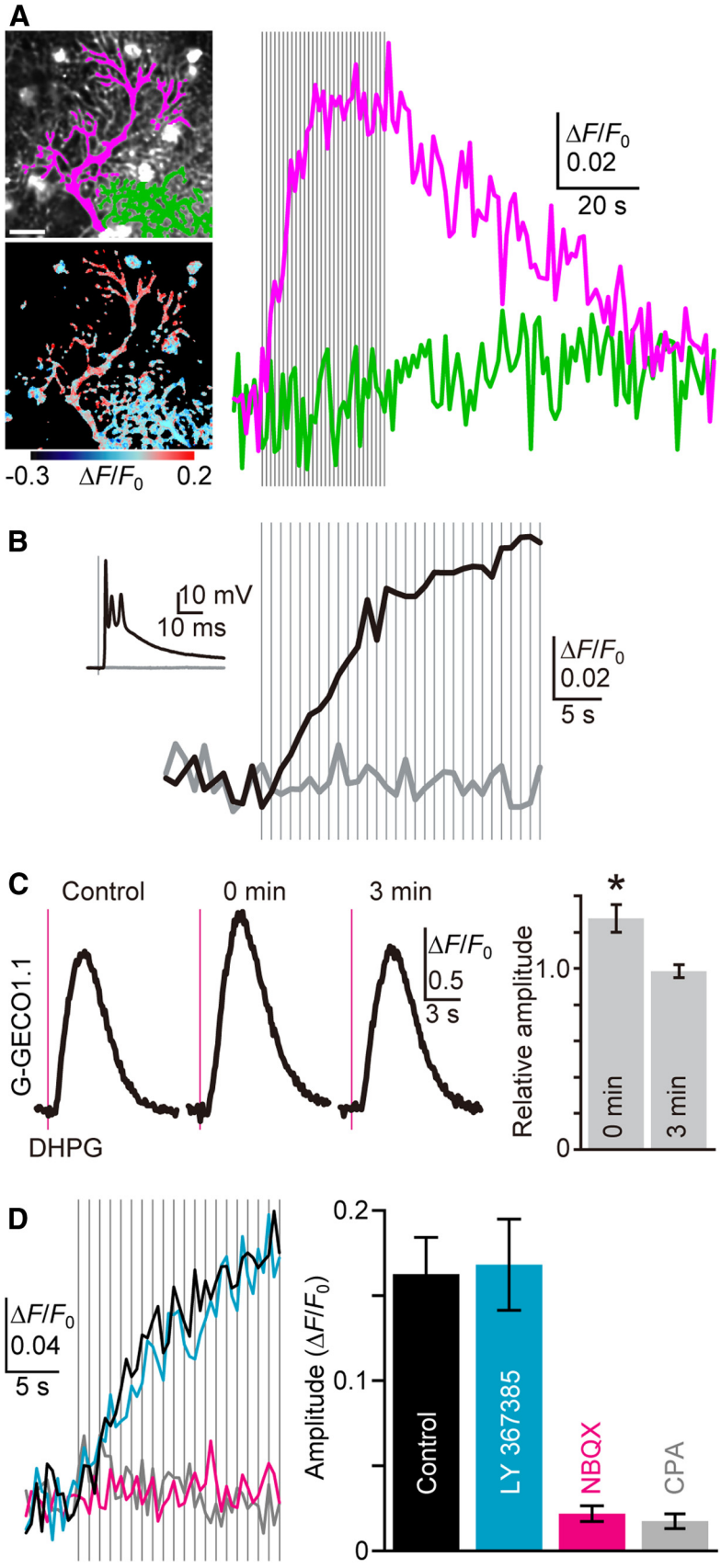

Figure 5. CF activity-induced ER Ca^{2+} overloading. ***A***, Representative time courses of mean $\Delta F/F_0$ throughout the dendrite of a stimulated PC (magenta in the top image, magenta trace) and a nonstimulated neighboring PC (green in the top image, green trace) upon repetitive CF inputs (30 stimuli at 1 Hz, gray vertical lines) indicate CF-induced ER Ca^{2+} dynamics in PCs. The pseudo-color image shows the average of 20 consecutive frames during CF stimulation. Scale bar, 20 μm. ***B***, CF stimulation (1 Hz, gray vertical lines) just above the threshold induced EPSP (black inset trace) and G-CEPIA1*er* response (black trace). In contrast, no EPSP (gray inset trace) and G-CEPIA1*er* responses (gray trace) were observed in the same PC upon stimulation just below the threshold. ***C***, Cytoplasmic Ca^{2+} measurement with G-GECO1.1. Ca^{2+} mobilization was induced by pressure ejection of DHPG (1 mM, 50 ms, 10–30 psi, magenta vertical line), either 5–10 s (0 min) or 3 min after CF stimulation (30 pulses at 1 Hz). Representative time courses of $\Delta F/F_0$ indicate the transient enhancement of mGluR1-induced Ca^{2+} mobilization after CF stimulation. The summarized bar graph for the amplitude of the responses normalized by the amplitude of the control is shown. $n = 7$ (mean ± SEM). *$p = 0.00559$, *t* test. ***D***, Pharmacological characterization of CF-induced ER Ca^{2+} dynamics. G-CEPIA1*er* responses upon CF inputs (1 Hz, gray vertical lines) in the control condition (black), or in the presence of LY367385 (100 μM, cyan), NBQX (10 μM, magenta), or CPA (50 μM, gray) are shown. Amplitude is defined as the maximum increase in $\Delta F/F_0$ during 20 pulses of CF stimulation. $n = 6$–13 (mean ± SEM).

limited contribution of SERCA to Ca^{2+} replenishment of the ER following PF stimulation-induced Ca^{2+} release.

The numerical simulation also predicted that if luminal Ca^{2+} diffusion is the main source of Ca^{2+} replenishment, the refilling rate will depend on the spatial distribution of areas of decreased $[Ca^{2+}]_{ER}$, such that the larger the area of $[Ca^{2+}]_{ER}$ decrease, the slower the rate of Ca^{2+} replenishment. In contrast, if the refilling mechanism is dominated by the activity of SERCA, the recovery rate will not depend on the amplitude and the spatial distribution of the areas of $[Ca^{2+}]_{ER}$ decrease. To distinguish between these possibilities, we analyzed the relationship between the spatial distribution of areas of $[Ca^{2+}]_{ER}$ decrease and the time course of recovery. We found that increasing the stimulation intensity by twofold resulted in increases in both the PF-induced Ca^{2+} depletion area and $t_{1/2}$ (Fig. 3*C–E*). We also observed that under conditions of elevated temperature, which enhance the activity of SERCA, there was a delay in the recovery of $[Ca^{2+}]_{ER}$ within the enlarged area of decreased $[Ca^{2+}]_{ER}$ (Fig. 3*E*). These results are consistent with the importance of luminal Ca^{2+} diffusion in Ca^{2+} replenishment.

Simultaneous replenishment of ER Ca^{2+} in dendrites and spines

In neurons, spine necks represent major barriers for cytoplasmic Ca^{2+} diffusion (Svoboda et al., 1996; Majewska et al., 2000; Sabatini et al., 2002; Hernjak et al., 2005; Noguchi et al., 2005), which raises the possibility that diffusion-dependent refilling of ER is impaired in spines. To address this question, we compared ER

Ca^{2+} dynamics between spines and their parent dendrites. We found that PF-induced G-CEPIA1*er* responses within the spines and their parent dendrites exhibited overlapping time courses (Fig. 4*A*). Moreover, following PF inputs, the dynamics of $[Ca^{2+}]_{ER}$ decrease (amplitude and time to peak) did not differ between these two cellular compartments (Fig. 4*B*), which is consistent with previous observations that, upon PF inputs, there are similarities in $[Ca^{2+}]_{cyt}$ transients in spines and dendrites (Finch and Augustine, 1998; Takechi et al., 1998). Furthermore, we observed no difference in the recovery rate ($t_{1/2}$) between spines and their parent dendrites (Fig. 4*B*). It has been shown that SERCA does not accumulate within spines (Takei et al., 1992); thus, the simultaneous recovery we observed supports the notion that spine necks do not represent rate-limiting barriers for diffusion-dependent Ca^{2+} replenishment in the ER. Earlier studies (Harris and Stevens, 1988; Martone et al., 1993) have suggested that, instead, the critical rate-limiting structure for intraluminal diffusion dynamics is a narrow cross section of the ER tubule found throughout the dendrites and spines.

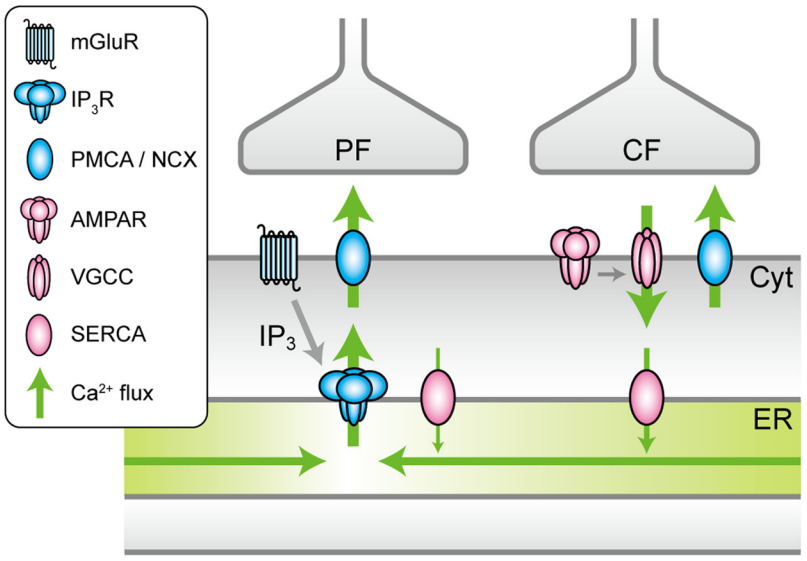

Figure 6. Schema of synaptically evoked Ca^{2+} flow in PCs. Schematic diagram showing Ca^{2+} flow in PCs upon PF and CF inputs. Ca^{2+} flow is mediated by channels, pumps, and diffusion. PF inputs induce local depletion of ER via mGluR1-IP_3 signaling, which is followed by the replenishment by intraluminal Ca^{2+} diffusion. CF inputs induce AMPAR-dependent Ca^{2+} spikes, which are followed by SERCA-dependent uptake of Ca^{2+} into the ER. Ca^{2+} in the ER lumen is exchanged between regions of relatively low and high $[Ca^{2+}]_{ER}$. PMCA, Plasma membrane Ca^{2+} ATPase; NCX, Na^+/Ca^{2+} exchanger; VGCC, voltage-gated Ca^{2+} channel.

CF inputs load the ER with Ca^{2+}

Previous studies have indicated that, in neurons, depolarization-induced Ca^{2+} influx can load the ER with Ca^{2+}, thereby potentiating subsequent Ca^{2+} mobilization (Brorson et al., 1991; Garaschuk et al., 1997; Finch and Augustine, 1998; Fiorillo and Williams, 1998; Stutzmann et al., 2003; Power and Sah, 2005; Hong and Ross, 2007; Hartmann et al., 2014). However, these studies did not directly measure $[Ca^{2+}]_{ER}$. Furthermore, whether physiologically relevant Ca^{2+} influx can increase $[Ca^{2+}]_{ER}$ is as yet unclear. CFs form strong synapses on PC dendrites in a one-to-one manner and induce large EPSPs followed by dendrite-wide Ca^{2+} spikes (Kitamura and Häusser, 2011). We found that repetitive CF stimulation using a physiologically relevant frequency (1 Hz) induced an accumulating increase in $[Ca^{2+}]_{ER}$ throughout the dendrite (Fig. 5*A*, magenta), but not in the adjacent nonstimulated PC (Fig. 5*A*, green). We observed no significant difference in the CF-induced $[Ca^{2+}]_{ER}$ elevation at different dendritic segments despite variations in CF-induced $[Ca^{2+}]_{cyt}$ transients that have been observed along PC dendrites (Otsu et al., 2014). We further confirmed the involvement of CFs by observing that there was a strict correlation between $[Ca^{2+}]_{ER}$ response and CF-EPSPs, in an all-or-none manner (Fig. 5*B*). CF-induced responses reached a plateau after 10–20 pulses of stimulation, likely because $[Ca^{2+}]_{ER}$ reached a new equilibrium during the repetitive Ca^{2+} spikes (Fig. 5*A*). Elevated $[Ca^{2+}]_{ER}$ levels returned to the basal level within a few minutes of the cessation of CF inputs, which is consistent with previous observations that the potentiating effect by the preceding depolarization lasted a few minutes (Brorson et al., 1991; Garaschuk et al., 1997; Stutzmann et al., 2003; Hong and Ross, 2007). Using cytoplasmic Ca^{2+} measurements, we confirmed that CF input trains, comprising 30 pulses at 1 Hz, enhanced subsequent mGluR1-mediated Ca^{2+} mobilization immediately after CF stimulation, but not 3 min after CF stimulation (Fig. 5*C*). This result is consistent with earlier studies showing that in PCs, depolarization potentiates the subsequent Ca^{2+} mobilization (Finch and Augustine, 1998; Hartmann et al., 2014). In this study, we observed both decreasing and increasing changes in the G-CEPIA1*er* fluorescence upon PF and CF inputs, suggesting that the basal $[Ca^{2+}]_{ER}$ is comparable with the dissociation constant of G-CEPIA1*er* (672 μM; Suzuki et al., 2014).

Next, we used pharmacological agents to determine which intracellular components are involved in CF-induced ER Ca^{2+} dynamics. NBQX blocks AMPA receptors, which are the major charge carriers at the CF–PC synapses. Thus, as expected, we found that NBQX blocked the CF-induced G-CEPIA1*er* response (Fig. 5*D*, magenta). In contrast, LY367385, which is an inhibitor of mGluR1, had no effect (Fig. 5*D*, cyan). The inhibition of SERCA by CPA abolished the G-CEPIA1*er* response, indicating that CF-induced Ca^{2+} influx was followed by SERCA-dependent uptake of Ca^{2+} into the ER (Fig. 5*D*, gray). In conclusion, we successfully visualized CF-induced ER filling and found evidence strongly suggesting that one function of the ER is as a leaky integrator of CF inputs.

Discussion

In this study, we successfully used G-CEPIA1*er* to visualize synaptic activity-evoked ER Ca^{2+} dynamics in central neurons, and detected the crucial contribution of intraluminal Ca^{2+} diffusion to replenishment of ER Ca^{2+} after PF-induced local decreases in $[Ca^{2+}]_{ER}$. We also demonstrated the involvement of CF-evoked Ca^{2+} spikes in the loading of Ca^{2+} into the ER. These results indicate that the neuronal ER functions as an intracellular Ca^{2+} tunnel that redistributes stored Ca^{2+} throughout dendritic arborizations, and as a leaky integrator of synaptic input trains. Thus, the G-CEPIA1*er*-based visualization method that we developed has allowed us to obtain a comprehensive understanding of synaptically evoked Ca^{2+} flux within the ER lumen and across the ER membrane of PCs (Fig. 6).

ER functions as a Ca^{2+} tunnel

Spatially confined local cytosolic Ca^{2+} signals have been observed within dendritic arborizations in response to synaptic inputs. Such localized cytosolic Ca^{2+} transients are realized due to the high Ca^{2+} buffering power of the cytoplasm, which restricts the diffusion of Ca^{2+}. In contrast, the ER comprises a Ca^{2+}-containing intracellular network that has been proposed to function as a "Ca^{2+} tunnel" for the transport of intracellular Ca^{2+}. The Ca^{2+} tunnel hypothesis has been previously tested under reduced experimental conditions, such as acutely isolated pancreatic acinar cells, cardiac myocytes, retinal photoreceptor cells, and dopamine neurons, in which $[Ca^{2+}]_{cyt}$ or $[Ca^{2+}]_{ER}$ is imaged after local application of either Ca^{2+} or Ca^{2+}-releasing reagents using fine pipettes or caged Ca^{2+} compounds (Mogami et al., 1997; Park et al., 2000; Choi et al., 2006; Wu and Bers, 2006; Swietach et al., 2008; Picht et al., 2011; Chen et al., 2015). In the current study, we provide strong support for the Ca^{2+} tunnel hypothesis based on the imaging of PCs under physiologically relevant conditions. Our data indicate that in PCs, the ER functions as a continuous Ca^{2+} reservoir in which Ca^{2+} is exchanged between Ca^{2+}-depleted and replete segments in response to repetitive PF inputs (Fig. 6).

Interestingly, we estimated that the effective Ca^{2+} diffusion coefficient within the ER along the dendrites (8.4 $\mu m^2/s$) was two orders of magnitude lower than the value for free diffusion of Ca^{2+} in water (~800 $\mu m^2/s$). This disparity is probably due to conditions in the ER such as a high concentration of Ca^{2+}-binding proteins (Pozzan et al., 1994), molecular crowding (Dayel et al., 1999), and the tortuosity of ER tubules (Harris and Stevens, 1988; Martone et al., 1993). It is noteworthy that the ER Ca^{2+} diffusion coefficient estimated in this study matches well with the value previously measured within the sarcoplasmic reticulum in cardiac myocytes (Swietach et al., 2008), although different values were reported by another group (Wu and Bers, 2006; Picht et al., 2011). According to our numerical simulation, despite the low Ca^{2+} diffusion coefficient within the ER, it still functions as an effective Ca^{2+} tunnel, due to the low Ca^{2+} pump and leak activities of the ER membrane. The ER Ca^{2+} diffusion coefficient that we estimated is comparable to or slightly lower than the value previously measured in the cytoplasmic extract (13 $\mu m^2/s$; Allbritton et al., 1992). However, PF-induced cytosolic Ca^{2+} transients are more spatially confined than the corresponding decreases in $[Ca^{2+}]_{ER}$ (Fig. 2*D*). The likely reason for the spatial restriction of the diffusion of cytosolic Ca^{2+} transients is that cytosolic Ca^{2+} is efficiently extruded through the plasma membrane. In line with this notion, studies have shown that, in terms of cytoplasmic Ca^{2+} clearance in central neurons, Ca^{2+} extrusion across the plasma membrane has a greater contribution than Ca^{2+} sequestration by SERCA (Fierro et al., 1998; Sabatini et al., 2002; Fig. 6).

ER as a memory of synaptic activity

The influx of Ca^{2+} across the plasma membrane is known to transiently potentiate subsequent Ca^{2+} release from stores within neurons (Brorson et al., 1991; Garaschuk et al., 1997; Stutzmann et al., 2003; Hong and Ross, 2007). Berridge (1998) hypothesized that this phenomenon is mediated by Ca^{2+} influx-dependent elevation of $[Ca^{2+}]_{ER}$, such that the ER functions as an integrator or "memory" of recent neuronal activities accompanying Ca^{2+} influx. In support of this hypothesis, we showed that 1 Hz CF inputs induce an accumulating increase in $[Ca^{2+}]_{ER}$, even though the decay of each CF stimulation-induced $[Ca^{2+}]_{cyt}$ transient had a fast time course relative to the 1 s interval (Kitamura and Häusser, 2011). Furthermore, the elevated $[Ca^{2+}]_{ER}$ lasted a few minutes after the cessation of CF inputs. Therefore, our data support the hypothesis that the ER of PCs can function as a leaky integrator, and the levels of $[Ca^{2+}]_{ER}$ reflect the recent history of CF inputs. Because CFs spontaneously and persistently fire at ~1 Hz in the cerebellum *in vivo*, the ER of PCs should be able to integrate CF-evoked Ca^{2+} spikes to persistently enhance SERCA-dependent filling mechanisms, even under basal conditions. Furthermore, since sensory inputs are known to evoke CF inputs, experience-dependent modulation of $[Ca^{2+}]_{ER}$ may be possible.

References

Allbritton NL, Meyer T, Stryer L (1992) Range of messenger action of calcium ion and inositol 1,4,5-trisphosphate. Science 258:1812–1815. CrossRef Medline

Berezhkovskii AM, Barzykin AV, Zitserman VY (2009) One-dimensional description of diffusion in a tube of abruptly changing diameter: boundary homogenization based approach. J Chem Phys 131:224110. CrossRef Medline

Berridge MJ (1998) Neuronal calcium signaling. Neuron 21:13–26. CrossRef Medline

Bonora M, Giorgi C, Bononi A, Marchi S, Patergnani S, Rimessi A, Rizzuto R, Pinton P (2013) Subcellular calcium measurements in mammalian cells using jellyfish photoprotein aequorin-based probes. Nat Protoc 8:2105–2118. CrossRef Medline

Brorson JR, Bleakman D, Gibbons SJ, Miller RJ (1991) The properties of intracellular calcium stores in cultured rat cerebellar neurons. J Neurosci 11:4024–4043. Medline

Chen M, Van Hook MJ, Thoreson WB (2015) Ca^{2+} diffusion through endoplasmic reticulum supports elevated intraterminal Ca^{2+} levels needed to sustain synaptic release from rods in darkness. J Neurosci 35:11364–11373. CrossRef Medline

Choi YM, Kim SH, Chung S, Uhm DY, Park MK (2006) Regional interaction of endoplasmic reticulum Ca^{2+} signals between soma and dendrites through rapid luminal Ca^{2+} diffusion. J Neurosci 26:12127–12136. CrossRef Medline

Dayel MJ, Hom EF, Verkman AS (1999) Diffusion of green fluorescent protein in the aqueous-phase lumen of endoplasmic reticulum. Biophys J 76:2843–2851. CrossRef Medline

Edwards FA, Konnerth A, Sakmann B, Takahashi T (1989) A thin slice preparation for patch clamp recordings from neurones of the mammalian central nervous system. Pflugers Arch 414:600–612. CrossRef Medline

Fierro L, DiPolo R, Llano I (1998) Intracellular calcium clearance in Purkinje cell somata from rat cerebellar slices. J Physiol 510:499–512. CrossRef Medline

Finch EA, Augustine GJ (1998) Local calcium signalling by inositol-1,4,5-trisphosphate in Purkinje cell dendrites. Nature 396:753–756. CrossRef Medline

Fiorillo CD, Williams JT (1998) Glutamate mediates an inhibitory postsynaptic potential in dopamine neurons. Nature 394:78–82. CrossRef Medline

Fujiwara A, Hirose K, Yamazawa T, Iino M (2001) Reduced IP_3 sensitivity of IP_3 receptor in Purkinje neurons. Neuroreport 12:2647–2651. CrossRef Medline

Garaschuk O, Yaari Y, Konnerth A (1997) Release and sequestration of calcium by ryanodine-sensitive stores in rat hippocampal neurones. J Physiol 502:13–30. CrossRef Medline

Harris KM, Stevens JK (1988) Dendritic spines of rat cerebellar Purkinje cells: serial electron microscopy with reference to their biophysical characteristics. J Neurosci 8:4455–4469. Medline

Hartmann J, Karl RM, Alexander RP, Adelsberger H, Brill MS, Rühlmann C, Ansel A, Sakimura K, Baba Y, Kurosaki T, Misgeld T, Konnerth A (2014) STIM1 controls neuronal Ca^{2+} signaling, mGluR1-dependent synaptic transmission, and cerebellar motor behavior. Neuron 82:635–644. CrossRef Medline

Hernjak N, Slepchenko BM, Fernald K, Fink CC, Fortin D, Moraru II, Watras J, Loew LM (2005) Modeling and analysis of calcium signaling events leading to long-term depression in cerebellar Purkinje cells. Biophys J 89:3790–3806. CrossRef Medline

Hong M, Ross WN (2007) Priming of intracellular calcium stores in rat CA1 pyramidal neurons. J Physiol 584:75–87. CrossRef Medline

Ishii K, Hirose K, Iino M (2006) Ca^{2+} shuttling between endoplasmic reticulum and mitochondria underlying Ca^{2+} oscillations. EMBO Rep 7: 390–396. CrossRef Medline

Kitamura K, Häusser M (2011) Dendritic calcium signaling triggered by spontaneous and sensory-evoked climbing fiber input to cerebellar Purkinje cells *in vivo*. J Neurosci 31:10847–10858. CrossRef Medline

Majewska A, Brown E, Ross J, Yuste R (2000) Mechanisms of calcium decay kinetics in hippocampal spines: role of spine calcium pumps and calcium diffusion through the spine neck in biochemical compartmentalization. J Neurosci 20:1722–1734. Medline

Makhnovskii YA, Berezhkovskii AM, Zitserman VY (2010) Diffusion in a tube of alternating diameter. Chem Phys 367:110–114. CrossRef

Martone ME, Zhang Y, Simpliciano VM, Carragher BO, Ellisman MH (1993) Three-dimensional visualization of the smooth endoplasmic reticulum in Purkinje cell dendrites. J Neurosci 13:4636–4646. Medline

Miyawaki A, Llopis J, Heim R, McCaffery JM, Adams JA, Ikura M, Tsien RY (1997) Fluorescent indicators for Ca^{2+} based on green fluorescent proteins and calmodulin. Nature 388:882–887. CrossRef Medline

Mogami H, Nakano K, Tepikin AV, Petersen OH (1997) Ca^{2+} flow via tunnels in polarized cells: recharging of apical Ca^{2+} stores by focal Ca^{2+} entry through basal membrane patch. Cell 88:49–55. CrossRef Medline

Noguchi J, Matsuzaki M, Ellis-Davies GC, Kasai H (2005) Spine-neck geometry determines NMDA receptor-dependent Ca^{2+} signaling in dendrites. Neuron 46:609–622. CrossRef Medline

Okubo Y, Kakizawa S, Hirose K, Iino M (2001) Visualization of IP_3 dynamics reveals a novel AMPA receptor-triggered IP_3 production pathway mediated by voltage-dependent Ca^{2+} influx in Purkinje cells. Neuron 32: 113–122. CrossRef Medline

Okubo Y, Kakizawa S, Hirose K, Iino M (2004) Cross talk between metabotropic and ionotropic glutamate receptor-mediated signaling in parallel fiber-induced inositol 1,4,5-trisphosphate production in cerebellar Purkinje cells. J Neurosci 24:9513–9520. CrossRef Medline

Otsu Y, Marcaggi P, Feltz A, Isope P, Kollo M, Nusser Z, Mathieu B, Kano M, Tsujita M, Sakimura K, Dieudonné S (2014) Activity-dependent gating of calcium spikes by A-type K^+ channels controls climbing fiber signaling in Purkinje cell dendrites. Neuron 84:137–151. CrossRef Medline

Palmer AE, Jin C, Reed JC, Tsien RY (2004) Bcl-2-mediated alterations in endoplasmic reticulum Ca^{2+} analyzed with an improved genetically encoded fluorescent sensor. Proc Natl Acad Sci U S A 101:17404–17409. CrossRef Medline

Park MK, Petersen OH, Tepikin AV (2000) The endoplasmic reticulum as one continuous Ca^{2+} pool: visualization of rapid Ca^{2+} movements and equilibration. EMBO J 19:5729–5739. CrossRef Medline

Petersen OH, Verkhratsky A (2007) Endoplasmic reticulum calcium tunnels integrate signalling in polarised cells. Cell Calcium 42:373–378. CrossRef Medline

Picht E, Zima AV, Shannon TR, Duncan AM, Blatter LA, Bers DM (2011) Dynamic calcium movement inside cardiac sarcoplasmic reticulum during release. Circ Res 108:847–856. CrossRef Medline

Power JM, Sah P (2005) Intracellular calcium store filling by an L-type calcium current in the basolateral amygdala at subthreshold membrane potentials. J Physiol 562:439–453. CrossRef Medline

Pozzan T, Rizzuto R, Volpe P, Meldolesi J (1994) Molecular and cellular physiology of intracellular calcium stores. Physiol Rev 74:595–636. Medline

Rodriguez-Garcia A, Rojo-Ruiz J, Navas-Navarro P, Aulestia FJ, Gallego-Sandin S, Garcia-Sancho J, Alonso MT (2014) GAP, an aequorin-based fluorescent indicator for imaging Ca^{2+} in organelles. Proc Natl Acad Sci U S A 111:2584–2589. CrossRef Medline

Sabatini BL, Oertner TG, Svoboda K (2002) The life cycle of Ca^{2+} ions in dendritic spines. Neuron 33:439–452. CrossRef Medline

Sharp AH, McPherson PS, Dawson TM, Aoki C, Campbell KP, Snyder SH (1993) Differential immunohistochemical localization of inositol 1,4,5-trisphosphate- and ryanodine-sensitive Ca^{2+} release channels in rat brain. J Neurosci 13:3051–3063. Medline

Solovyova N, Veselovsky N, Toescu EC, Verkhratsky A (2002) Ca^{2+} dynamics in the lumen of the endoplasmic reticulum in sensory neurons: direct visualization of Ca^{2+}-induced Ca^{2+} release triggered by physiological Ca^{2+} entry. EMBO J 21:622–630. CrossRef Medline

Stutzmann GE, LaFerla FM, Parker I (2003) Ca^{2+} signaling in mouse cortical neurons studied by two-photon imaging and photoreleased inositol triphosphate. J Neurosci 23:758–765. Medline

Suzuki J, Kanemaru K, Ishii K, Ohkura M, Okubo Y, Iino M (2014) Imaging intraorganellar Ca^{2+} at subcellular resolution using CEPIA. Nat Commun 5:4153. CrossRef Medline

Svoboda K, Tank DW, Denk W (1996) Direct measurement of coupling between dendritic spines and shafts. Science 272:716–719. CrossRef Medline

Swietach P, Spitzer KW, Vaughan-Jones RD (2008) Ca^{2+}-mobility in the sarcoplasmic reticulum of ventricular myocytes is low. Biophys J 95:1412–1427. CrossRef Medline

Takechi H, Eilers J, Konnerth A (1998) A new class of synaptic response involving calcium release in dendritic spines. Nature 396:757–760. CrossRef Medline

Takei K, Stukenbrok H, Metcalf A, Mignery GA, Südhof TC, Volpe P, De Camilli P (1992) Ca^{2+} stores in Purkinje neurons: endoplasmic reticulum subcompartments demonstrated by the heterogeneous distribution of the InsP3 receptor, Ca^{2+}-ATPase, and calsequestrin. J Neurosci 12: 489–505. Medline

Tang S, Wong HC, Wang ZM, Huang Y, Zou J, Zhuo Y, Pennati A, Gadda G, Delbono O, Yang JJ (2011) Design and application of a class of sensors to monitor Ca^{2+} dynamics in high Ca^{2+} concentration cellular compartments. Proc Natl Acad Sci U S A 108:16265–16270. CrossRef Medline

Verkhratsky A (2005) Physiology and pathophysiology of the calcium store in the endoplasmic reticulum of neurons. Physiol Rev 85:201–279. CrossRef Medline

Wu J, Prole DL, Shen Y, Lin Z, Gnanasekaran A, Liu Y, Chen L, Zhou H, Chen SR, Usachev YM, Taylor CW, Campbell RE (2014) Red fluorescent genetically encoded Ca^{2+} indicators for use in mitochondria and endoplasmic reticulum. Biochem J 464:13–22. CrossRef Medline

Wu X, Bers DM (2006) Sarcoplasmic reticulum and nuclear envelope are one highly interconnected Ca^{2+} store throughout cardiac myocyte. Circ Res 99:283–291. CrossRef Medline

Zhao Y, Araki S, Wu J, Teramoto T, Chang YF, Nakano M, Abdelfattah AS, Fujiwara M, Ishihara T, Nagai T, Campbell RE (2011) An expanded palette of genetically encoded Ca^{2+} indicators. Science 333:1888–1891. CrossRef Medline